PNAS
www.pnas.org

Supplementary Information for
Highly Reversible Zn Metal Anode Enabled by Sustainable Hydroxyl Chemistry

Lin Ma[1,7,§*], Jenel Vatamanu[1§], Nathan T. Hahn[2], Travis P. Pollard[1], Oleg Borodin[1*], Valeri Petkov[3], Marshall A. Schroeder[1], Yang Ren[4], Michael S. Ding[1], Chao Luo[5*], Jan L. Allen[1], Chunsheng Wang[6], Kang Xu[1*]

[1] Battery Science Branch, Energy Science Division, Sensor and Electron Devices Directorate, DEVCOM Army Research Laboratory, Adelphi, MD 20783, USA
[2] Material, Physical and Chemical Sciences Center, Sandia National Laboratories, Albuquerque, NM 87185, USA
[3] Department of Physics, Central Michigan University, Mount Pleasant, Michigan 48859, USA
[4] Advanced Photon Source, Argonne National Laboratory, Lemont, IL 60439, USA
[5] Chemistry & Biochemistry Department, George Mason University, Fairfax, VA 22030, USA
Quantum Science & Engineering Center, George Mason University, Fairfax, VA, 22030, USA
[6] Department of Chemical and Biomolecular Engineering, University of Maryland, College Park, MD 20742, USA
[7] Department of Mechanical Engineering and Engineering Science, The University of North Carolina at Charlotte, Charlotte, NC, 28223, USA

[§]These authors contributed equally
*Corresponding author,
Email: l.ma@uncc.edu; oleg.a.borodin.civ@army.mil; cluo@gmu.edu; conrad.k.xu.civ@army.mil

This PDF file includes:

- Methods and Materials
- Figures S1. Deconvolution results of Raman spectra.
- Figures S2. A summary of electrolyte permittivity measured using DSR
- Figures S3. Dielectric loss spectrum of selected electrolytes
- Figures S4. Summary of MeOH contribution to dielectric relaxation from MD simulations
- Figures S5. Structure of pure MeOH and MeOH-ZnOTF electrolytes was analyzed using MD simulations and X-ray measurements

- Figures S6. Summary of CIP percentage in different electrolytes based on MD simulation results
- Figures S7. MD simulation results for different electrolytes
- Figures S8. pH testing
- Figures S9. Exemplar results of Zn^{2+} transference number testing process**.**
- Figures S10. Summary of viscosity and Walden plots.
- Figures S11. Zn plating/stripping CE screening testing results at room temperature
- Figures S12. Zn plating/stripping CE testing results
- Figures S13. Zn plating/stripping CE testing results.
- Figures S14. Symmetric cell screening testing results
- Figures S15. Symmetric cell screening testing results
- Figures S16. Zn plating/stripping CE screening testing results at -40°C
- Figures S17. Zn plating/stripping CE testing results at -40°C.
- Figures S18. Nyquist plots for Zn|Zn (100 μm) cells with selected electrolytes at different cycling time and different temperatures
- Figures S19. XPS spectra of $Zn(OTf)_2$ salt
- Figures S20. Depth profile of XPS spectra
- Figures S21. A summary of image snapshot with side and frontal view of the electrode-electrolyte interface
- Figures S22. DFT calculations on OTf^- anion reduction potential in a MeOH environment
- Figures S23. DFT calculations on hydrogen evolution and reduction with dissolved oxygen in a MeOH environment
- Figures S24. Depth profile of XPS spectra
- Figures S25. Depth profile of XPS spectra
- Figures S26. Depth profile of XPS spectra
- Figures S27. Zn interphase morphology and chemistry during cycling
- Figures S28. Zn interphase morphology and chemistry during cycling
- Figures S29. Nucleophilic attack by methoxide on triflate, chemical decomposition in implicit solvent represented using PCM(acetone)/M05-2X/6-311++G(3df,3pd) method
- Figures S30. DFT calculations on OTf^- anion reduction on a nano-scale ZnO cluster distributed on Zn metal surface using PCM(acetone)/M05-2X/6-31+G(d,p) method
- Figures S31. XPS spectra of pristine Zn foil
- Figures S32. XRD pattern of Zn metal electrodes
- Figures S33. Leakage/corrosion current testing with selected electrolytes during open circuit voltage condition at room temperature
- Figures S34. Zn reversibility in EtOH:$Zn(OTf)_2$ 111:1 by mol electrolyte at room temperature
- Figures S35. XPS spectra on Zn metal anode
- Figures S36. The effect of water on Zn reversibility in MeOH:$Zn(OTf)_2$ 14:1 by mol electrolyte at room temperature
- Figures S37. Electrochemical stability analysis of the selected Zn electrolytes at room temperature
- Figures S38. Long-term cycling details at 30°C
- Figures S39. Long-term cycling details at -40°C
- Figures S40. Zn reversibility in green salt containing electrolyte at room temperature
- Figures S41. Full cell performance demonstration of MeOH-based electrolytes
- Figures S42. Methanol hexamer geometry used for estimating the free energy of methanol monomer in bulk methanol
- Figures S43. Image snapshots of optimized clusters with molecular mechanics
- Figures S44. Typical setup for the electrode-electrolyte simulations, consisting of an electrolyte confined between two oppositely charged electrodes
- Tables S1. Summary of Zn metal anode reversibility in selected state-of-art Zn electrolyte at room temperature or low temperature (<0°C)
- Tables S2. Summary of MD simulation results on H-bond in different electrolytes.

- Tables S3. A summary of MD simulations of $Zn(OTf)_2$ in MeOH at 60 °C
- Tables S4. Summary of cell energy density estimation for Figure 4 at 30°C.
- Tables S5. A summary of estimated cost (per kg) for selected state-of-art electrolytes.
- Tables S6. Binding energies of various clusters in vacuum calculated with molecular mechanics (MM) using developed force field and quantum chemistry (QC).
- Tables S7. The revised OTF^- parameters used in MD simulations of MeOH/$Zn(OTf)_2$ electrolytes

Methods and Materials

Electrochemical measurements

2032-type coin cells were fabricated for all the Cu|Zn, Zn|Zn and PANI|Zn cells shown in this work. In each cell setup, 150 μL electrolyte was filled to fully wet the separator-a piece of Whatman Quartz Microfiber (QM-A). All the Cu|Zn and Zn|Zn cells were prepared in an Ar-filled glovebox and PANI|Zn cells were fabricated in a dry room (dew point -30°C or better). All the cells were tested with a Maccor cycler. Cu|Zn cell setup with two thickness of Zn foil electrode (100 μm and 10 μm) was used to leverage Zn plating/stripping Coulombic efficiency (CE). During the initial screening testing process, Cu|Zn (100 μm) cells were tested according to the protocol reported by previous work(1). Prior to Zn plating/stripping step, Cu electrode was conditioned by plating (0.5 mA cm^{-2}, 5 mAh cm^{-2}) and stripping Zn (0.5 V), and then covered by a Zn reservoir with a capacity of 5 mAh cm^{-2} (Q_t) using 0.5 mA cm^{-2}. Then Zn was plated and stripped during the following 9 cycles with 0.5 mA cm^{-2}, 1mAh cm^{-2} (Q_c) in each cycle. A final capacity (Q_s) was achieved when plated Zn was stripped by charging to 0.5 V in the last step. The average CE result is calculated according to equation S1:

$$CE = \frac{9Qc+Qs}{9Qc+Qt} \qquad \text{equation S1}$$

Towards the direction of practical application, Cu|Zn (10 μm) cell setup was adopted for leveraging CE of selected electrolyte systems. During each cycle, Zn was plated on Cu electrode by discharging the cell with two conditions: 1.17 mA cm^{-2}, 1.17 mAh cm^{-2} (Q_p, 20% utilization per cycle) at -40°C or 2.93 mA cm^{-2}, 2.93 mAh cm^{-2} (Q_p, 50% utilization per cycle) at room temperature, then Zn was stripped by charging the cell to 0.5 V (Q_s). CE per cycle is calculated based on equation S2:

$$CE = \frac{Qs}{Qp} \qquad \text{equation S2}$$

Zn|Zn (100 μm) symmetric cell testing was conducted with three conditions: 1 mA cm^{-2}, 1 mAh cm^{-2}; 2.5 mA cm^{-2}, 2.5 mAh cm^{-2}; and 1 mA cm^{-2}, 5 mAh cm^{-2} per charge/discharge step at room temperature. PANI|Zn (10 μm) full cells were tested with 60 mA g^{-1} or 360 mA g^{-1} (based on HNVO mass) at both 30°C (0.4-1.4V) and -40°C (0.4-1.8V). Five cycles between 0.4 and 0.9 V is necessary for activation purpose prior to long term cycling. EIS measurements were performed on Zn|Zn (100 μm) symmetric cells with selected electrolytes at zero state of charge. All the spectra were obtained with ten points per decade from 100 kHz to 10 mHz with a signal amplitude of 10 mV at room temperature by using a single-channel Gamry Potentiostat (Reference 3000). Electrochemical stability window of selected electrolytes was tested using a three-electrode Swagelok cell setup connected to a single channel Gamry Potentiostat (Reference 3000). The three-electrode cell setup consists of a stainless steel (SS) rod as the working electrode, carbon black as the counter electrode and Ag/AgCl as the reference electrode. The measurements were carried out with a scan rate of 5mV s^{-1} at room temperature within different voltage ranges: -1 V to 0 V for cathodic region; 0 V to 1.8 V for anodic region.

Computational methods

Reactivity and reduction potentials

Reaction free energies for alkoxide – OTf^- species were computed at the PCM(acetone)/M052X/6-311++G(3df,3pd) level of theory.(2) Reduction potentials were computed always with the

PCM(acetone)/M052X method for $[ZnOTf(MeOH)_5]^+$ cluster, though with differing basis sets: 1) sampling dozens of especially product (C-S, C-F cleavage) configurations with 6-31+G(d,p), 2) additional sampling mixing newly generated configurations and the best ones from the previous step with 6-31++G(2d,2p), and 3) a mix of top performers from the previous step with 6-311++G(3df,3pd). It was assumed the final product would retain octahedral geometry to avoid errors with implicit solvation due to changes in coordination number. To assist in this process (and increase computational speed), the reduced species were $[ZnOTf(MeOH)_4]^+$ and the 5th methanol was assumed to return to a bulk reservoir. The free energy of bulk methanol was estimated as $^1/_6$ the free energy of cyclic hexamer geometry computed always with the same basis as the Zn^{2+} cluster (Fig. S41). Malloum et al.(3) demonstrated the cyclic cluster to be strongly dominant across a broad temperature range relative to other hexamer structures, hence this is the only structure we've considered. All calculations have been performed in Gaussian 16 rev C01 and we used Atomic Simulation Environment for the preparation of all Gaussian files.(4, 5) Geometries were built in Avogadro(6) and used a combination of free or partially constrained optimization with the MMFF94 force field(7) and some additional hand optimization. Configurations with both small and large reorganizations upon reduction were considered, typically those with larger reorganization were thermodynamically preferred, though they can be reasonably expected to occur on longer time scales. PCM(ε=20, acetone) implicit solvent model was used. The reduced dielectric constant used in the PMC model reflects conditions common to moderately to highly concentrated battery electrolytes. Reaction free energies are computed as differences in the free energies for the optimized structures of [products] – [reactants] and the reduction potentials were computed from free energy differences in the optimized structures of the reduced species A^- and non-reduced species A via,

$$E^{red} = -\frac{[\Delta G(A^-) + \Delta G(MeOH) - \Delta G(A)]}{nF} - 3.68 \text{ V}$$

where, n is the number of electrons, F is Faraday's constant, the free energies are in units of Hartree (convert directly to eV multiplying by a factor of 27.2114, which is equivalent to conversion to kcal mol^{-1} and division by F as 23.061 kcal mol^{-1} V^{-1}, with minor differences due to rounding), and the 3.68 V shift reflects a shift to the Zn scale, assuming 4.44 V for the absolute potential of the standard hydrogen electrode.(8) This shift intrinsically depends on the absolute single ion solvation free energy of the proton (for SHE potential) and the electrochemically active cation in a given solvent, which could vary in the range of upwards of ± 0.3 V, possibly more. The middle term in the numerator above is the average free energy for a single methanol from the hexamer structure as discussed previously. Some spot checks were run with an explicit 5th methanol in the second solvation shell, the potentials are within ~0.1 V of the same structure with only the first shell molecules included. This is sensible given that the bulk energy is computed from a cyclic structure featuring hydrogen bonding and when explicitly considered, the 5th methanol typically hydrogen bonds to one of the anion fragments. The results are most meaningful when combined with characterization of the electrode surface.

pKa calculations using the method of Bryantsev(9) were performed at the M052X/6-311++G(3df,3pd) level of theory with some sampling of implicit solvation model used (PCM vs SMD) and the solvent considered. Acetone (reduced dielectric) and methanol were considered as well as DMSO to facilitate comparison to previously predicted pKa values from Kelly et al.(10) Proton solvation free energies in methanol were taken from Kelly et al and Malloum et al.(3, 10) All values are reported using the Malloum figure for the proton solvation free energy, add 0.3 to each reported pKa to convert to the Kelly result.

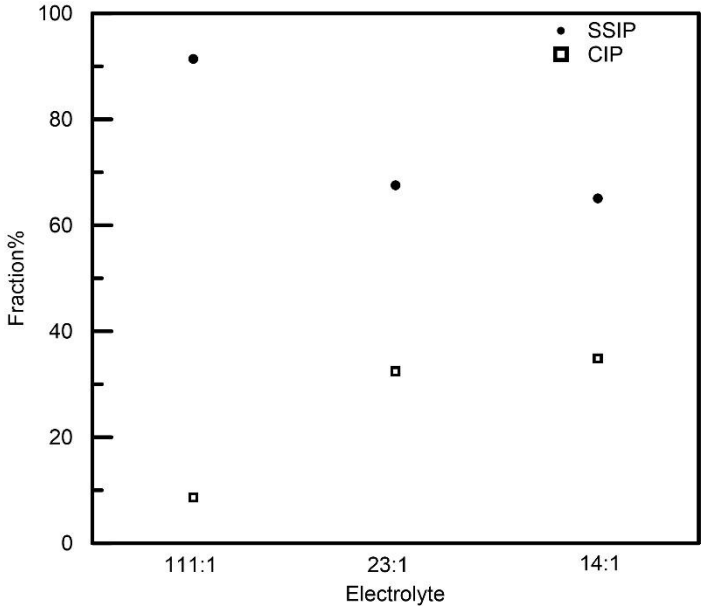

Fig. S1. Deconvolution results of Raman spectra. Summary of the respective fractions of free ions or SSIP and CIP of the OTf^- anion in MeOH based on the Gaussians deconvolution of Raman spectra. Corresponding Raman spectra is shown in Figure 1A-C.

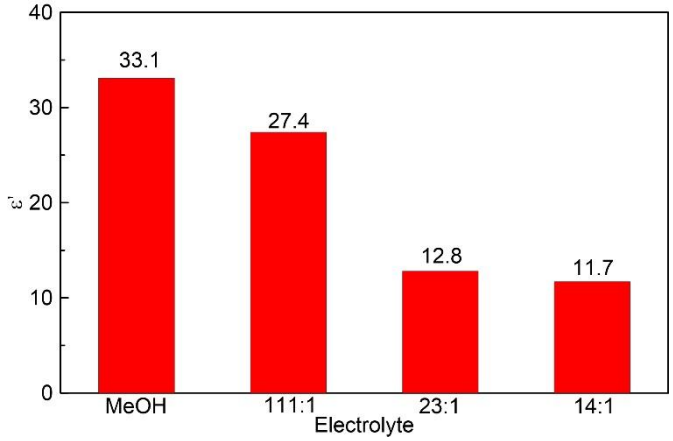

Fig. S2. A summary of electrolyte permittivity measured using DRS. Corresponding spectra is shown in Figure 1D.

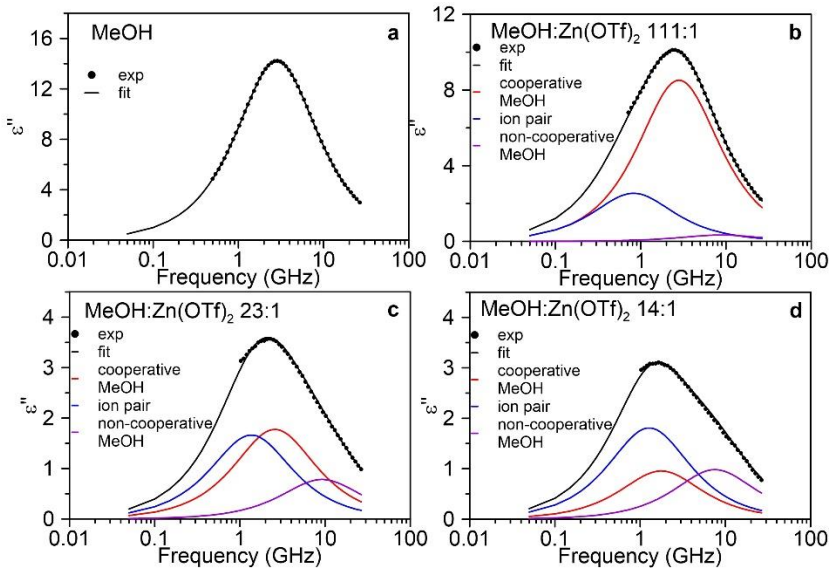

Fig. S3. Dielectric loss spectrum of selected electrolytes. a, MeOH; **b,** MeOH:$Zn(OTf)_2$ 111:1 by mol; **c,** MeOH:$Zn(OTf)_2$ 23:1 by mol; **d,** MeOH:$Zn(OTf)_2$ 14:1 by mol at 25 °C. Deconvoluted parts are shown in each panel.

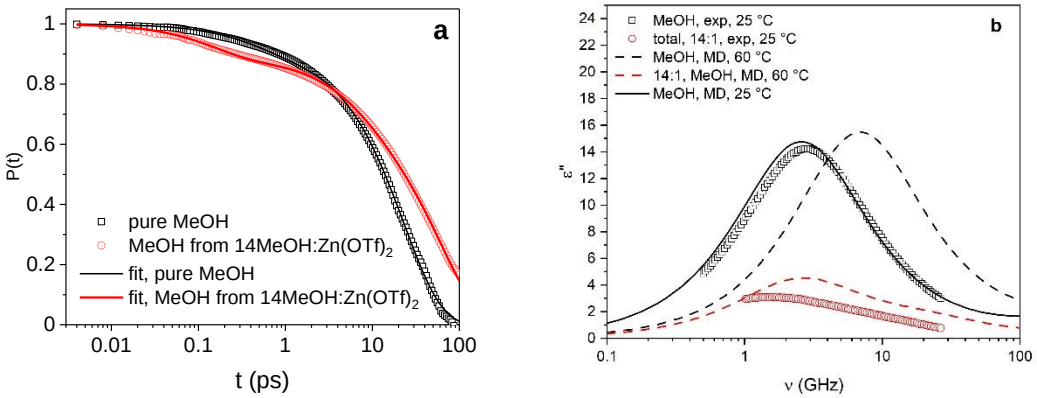

Fig. S4. Summary of MeOH contribution to dielectric relaxation from MD simulations: a, dipole moment autocorrelation function P(t) for pure MeOH and all MeOH molecules in 14:1 MeOH:$Zn(OTf)_2$ at 60 °C and the corresponding fits by a sum of 2 and 3 exponentials; **b,** dielectric loss from MD simulations and experiments. MD data at 25°C was scaled by 0.8 to match the height of experimental spectra.

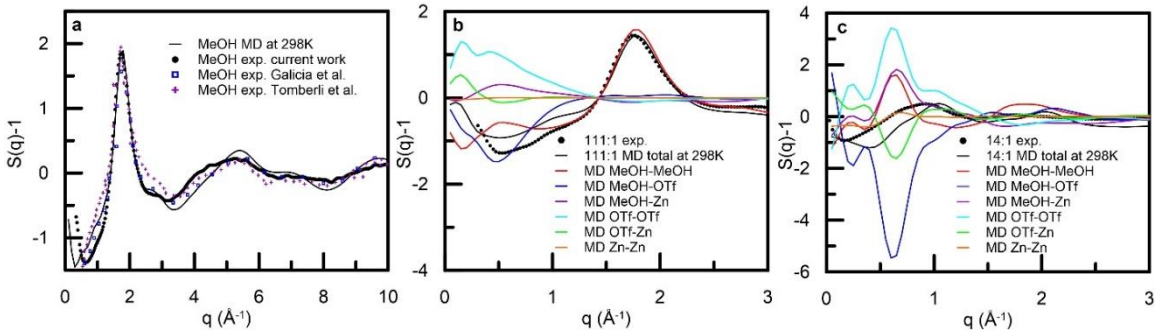

Fig. S5. Structure of pure MeOH and MeOH-ZnOTF electrolytes was analyzed using MD simulations and X-ray measurements. a, Structure factor of pure MeOH at 298 K from MD simulations, current X-ray experiments compared to previously reported X-ray measurements by Tomberli et al.(11) and Galicia-Andrés et al.(12). **b-c,** Contributions from solvent and ions correlations to structure factor obtained from MD simulations for **b,** 111:1 and **c,** 14: 1 electrolytes, respectively.

MD simulations adequately predict S(q) with some deviations observed between 3 and 5Å^{-1} for pure MeOH in **a**. Addition of small amount of salt (111:1 electrolyte) has only minor influence on the first intermolecular peak around 1.9 Å^{-1} **b,** compared to pure MeOH due to small contributions from everything but MeOH-MeOH for q>1.5 Å as shown in **b**. The MeOH-OTF and OTF-OTF contributions become more significant at lower q-values but largely cancel each other resulting in only minor deviations of the total S(q) from the MeOH-MeOH partial. A new small peak of the MeOH-MeOH partial at 0.5 Å^{-1} appears that is not present in pure liquid. It is attributed to the MeOH-MeOH correlations for the solvated $Zn(MeOH)_6$.

Further addition of salt to 14:1 concentration leads to a large shift in structure factor first intermolecular peak from 1.9 Å^{-1} to a much smaller q of 1.0 Å^{-1} **c,**. A new large peak at 0.6 Å^{-1} appeared in the MeOH-MeOH contribution that is attributed to MeOH-MeOH correlations in the $Zn(MeOH)_6$, while a second MeOH-MeOH around 1.8 Å^{-1} become broader compared to pure MeOH indicating disruption of the MeOH-MeOH intermolecular structure. In addition to MeOH-MeOH, the OTF-OTF correlations result in a large positive contribution around 0.6 Å^{-1} that are partially cancelled by the large negative contributions by MeOH-OTF and OTF-Zn. The first peak in total S(q) is due to OTF-OTF with smaller contributions due to MeOH-Zn and Zn-OTF, while MeOH-OTF has a negative contribution at this region.

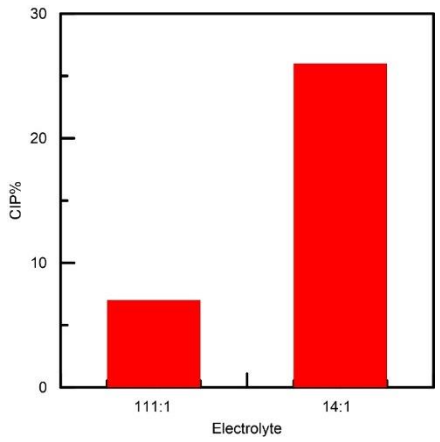

Fig. S6. Summary of CIP percentage in different electrolytes based on MD simulation results. a, MeOH:Zn(OTf)$_2$ 111:1 by mol; **b,** MeOH:Zn(OTf)$_2$ 14:1 by mol. %Zn of CIP was calculated based on Zn-S distance (4.2 Å) or Zn-O distance (3.0 Å).

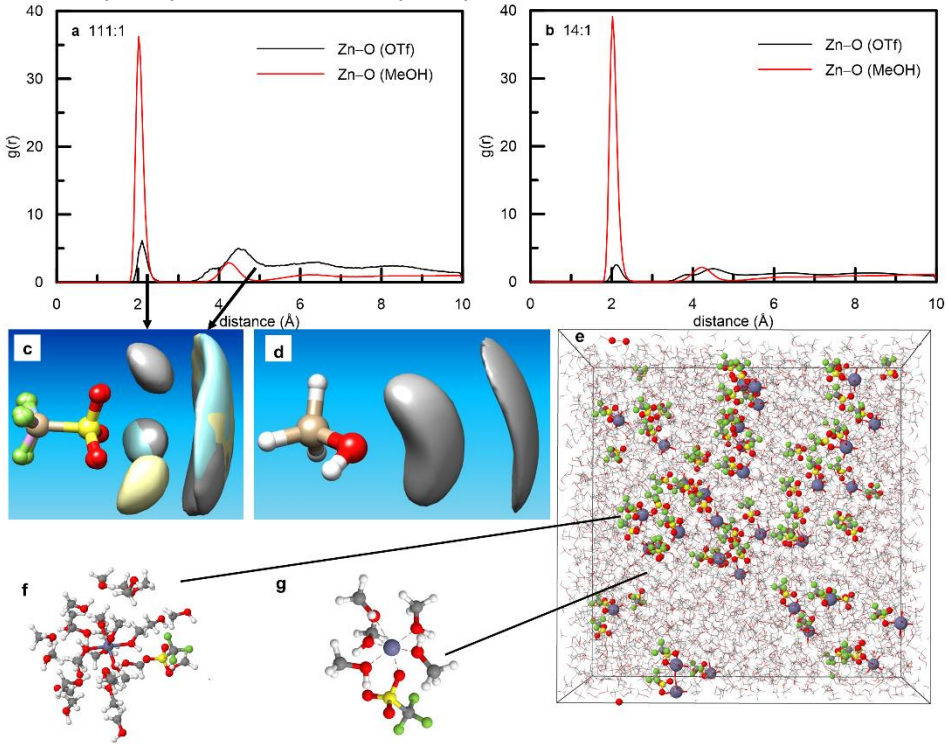

Fig. S7. MD simulation results for different electrolytes. a-b, The radial distribution function (RDF) of Zn-O/OTf vs Zn-O/MeOH for **a,** MeOH:Zn(OTf)$_2$ 111:1 by mol and **b,** MeOH/Zn(OTf)$_2$ 14:1 by mol electrolyte, respectively. Note that $(Zn(MeOH)_6)^{2+}$ solvates are long lived with the residence time 42 ns and 38 ns for 111:1 and 14:1 composition, respectively, at 60 °C. **c-d,** Isosurfaces for Zn around MeOH (ρ/ρ_{bulk} =13) and OTF anions (ρ/ρ_{bulk} =12) showing the most probable location of Zn near MeOH and OTF for MeOH:Zn(OTf)$_2$ 111:1 by mol. **e,** Snap-shot from MeOH:Zn(OTf)$_2$ 111:1 by mol electrolyte with **f,** SSIP and **g,** CIP configurations.

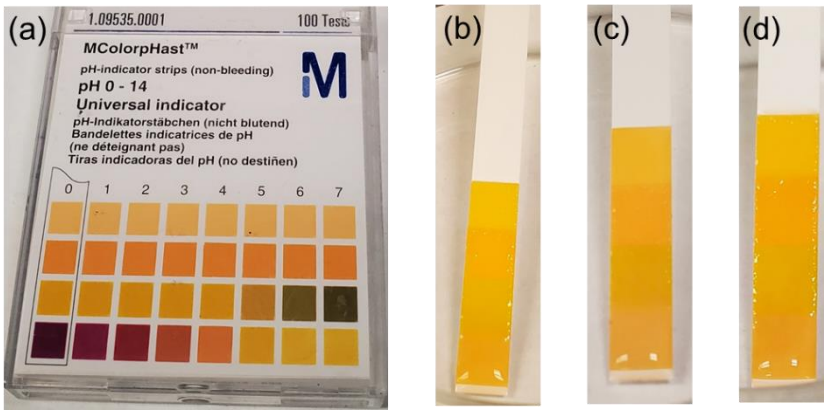

Fig. S8. pH testing. a, pH paper. Testing results for different electrolytes: **b,** MeOH:$Zn(OTf)_2$ 111:1 by mol; **c,** 23:1 by mol and **d,** 14:1 by mol.

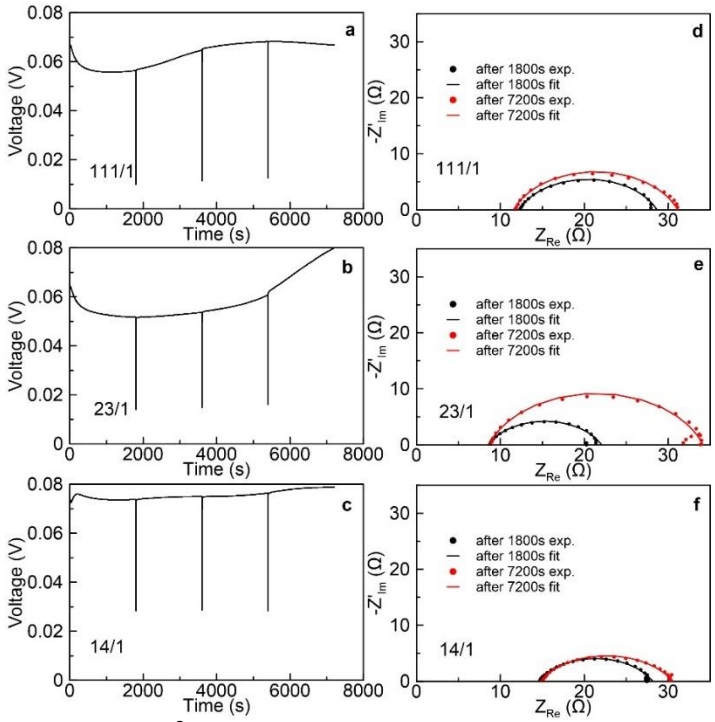

Fig. S9. Exemplar results of Zn^{2+} transference number testing process. a-c, Voltage vs. time for Zn|Zn cells during galvanostatic polarization process with 4 mA cm^{-2} at room temperature with three selected electrolytes as labeled in each panel. AC impedance spectra were collected every 1800s. **d-f,** Representative AC impedance spectra measured after 1800s and 7200s polarization process with three selected electrolytes as labeled in each panel. Fitted curves are also included.

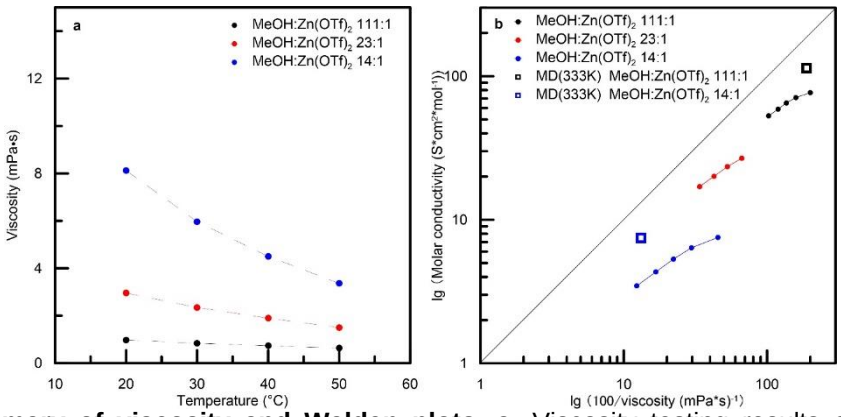

Fig. S10. Summary of viscosity and Walden plots. a, Viscosity testing results of selected electrolytes. **b,** Walden plot for selected electrolytes.

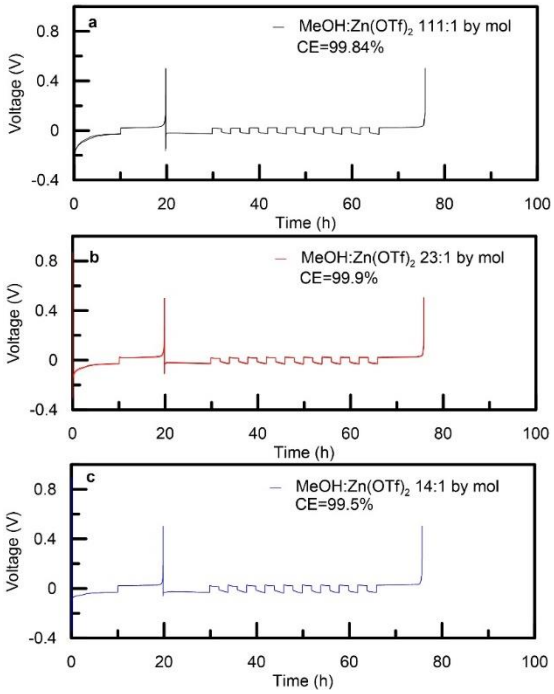

Fig. S11. Zn plating/stripping CE screening testing results at room temperature. Voltage vs time for Cu|Zn (100 μm) cells at room temperature with selected electrolytes as labeled in **a-c.** Cu was conditioned by plating (0.5 mA cm^{-2}, 5 mAh cm^{-2}) and stripping Zn (0.5 V) during the first cycle. Then a Zn reservoir with a capacity of 5 mAh cm^{-2} was built on the Cu substrate by using the same current density used for the following cycling. 0.5 mA cm^{-2} was used for stripping and plating Zn during the following 9 cycles. A capacity of 1mAh cm^{-2} (Q_c) Zn was plated or stripped in each cycle. In the final step, a capacity was observed when plated Zn was stripped by charging to 0.5 V. Calculated Zn plating/stripping CE were labeled in each panel.

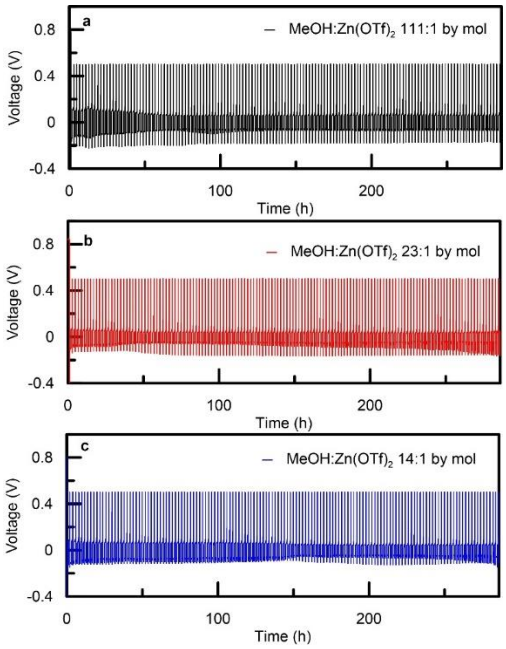

Fig. S12. Zn plating/stripping CE testing results. Voltage vs time for Cu|Zn (10 μm) cells (2.93 mA cm^{-2}, 2.93 mAh cm^{-2} and 50% Zn utilization per cycle) were used to plate Zn on Cu substrate, then charged to 0.5 V to strip Zn at room temperature with different electrolytes as labeled in each panel shown in **a-c**. Corresponding average CEs have been shown in Figure 2A-C.

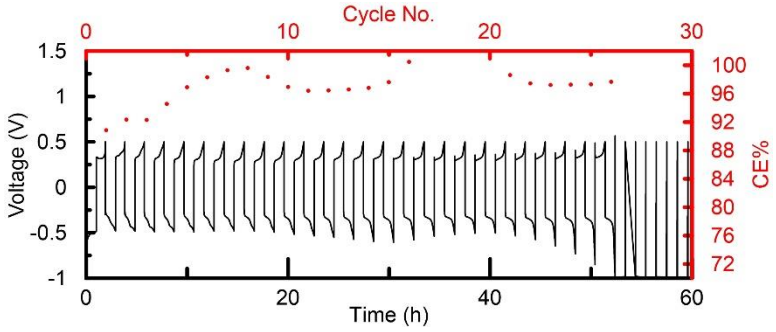

Fig. S13. Zn plating/stripping CE testing results. Voltage vs. time and corresponding CE vs. cycle No. for Cu|Zn (10 μm) cells (2.93 mA cm^{-2}, 2.93 mAh cm^{-2} and 50% Zn utilization per cycle) were used to plate Zn on Cu substrate, then charged to 0.5 V to strip Zn at room temperature with state-of-art non-aqueous electrolyte: 0.5M $Zn(OTf)_2$ in TEP.

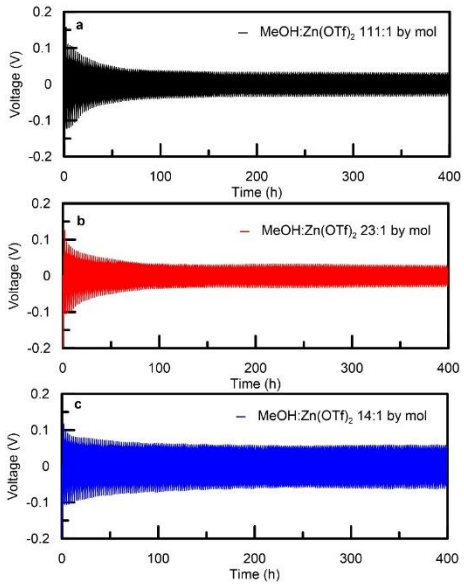

Fig. S14. Symmetric cell screening testing results. Voltage vs time for Zn|Zn (100 μm) symmetric cells (1 mA cm^{-2}, 1 mAh cm^{-2} per cycle) at room temperature with different electrolytes as labeled in **a-c**.

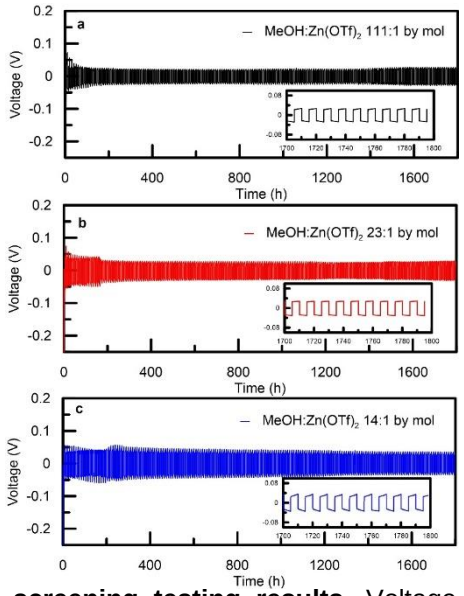

Fig. S15. Symmetric cell screening testing results. Voltage vs time for Zn|Zn (100 μm) symmetric cells (1 mA cm^{-2},5 mAh cm^{-2} per cycle) at room temperature with different electrolytes as labeled in **a-c**.

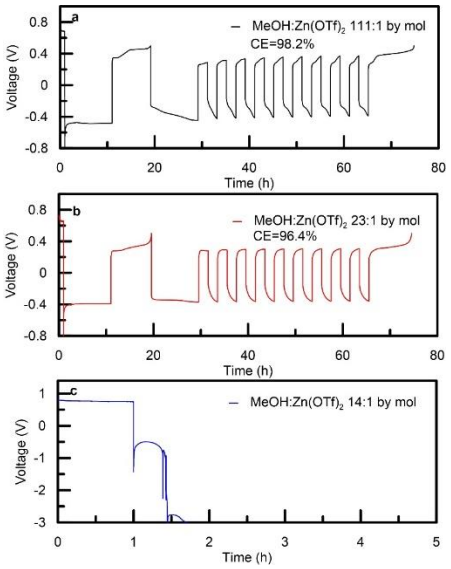

Fig. S16. Zn plating/stripping CE screening testing results at -40°C. Voltage vs time for Cu|Zn (100 μm) cells at room temperature with selected electrolytes as labeled in **a-c**. Cu was conditioned by plating (0.5 mA cm^{-2}, 5 mAh cm^{-2}) and stripping Zn (0.5 V) during the first cycle. Then a Zn reservoir with a capacity of 5 mAh cm^{-2} was built on the Cu substrate by using the same current density used for the following cycling. 0.5 mA cm^{-2} was used for stripping and plating Zn during the following 9 cycles. A capacity of 1mAh cm^{-2} (Q_c) Zn was plated or stripped in each cycle. In the final step, a capacity was observed when plated Zn was stripped by charging to 0.5 V. Calculated Zn plating/stripping CE were labeled in each panel.

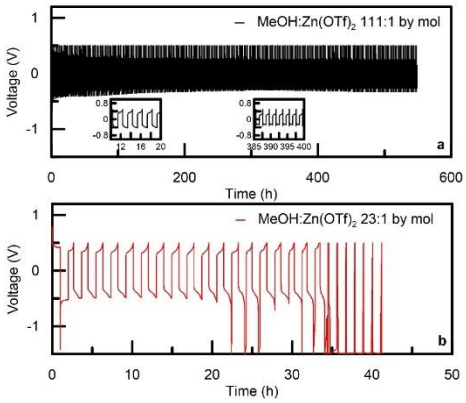

Fig. S17. Zn plating/stripping CE testing results at -40°C. Voltage vs time for Cu|Zn (10 μm) cells (1.17 mA cm^{-2}, 1.17 mAh cm^{-2} and 20% Zn utilization per cycle) were used to plate Zn on Cu substrate, then charged to 0.5 V to strip Zn at -40°C with different electrolytes as labeled in each panel shown in **a-b**.

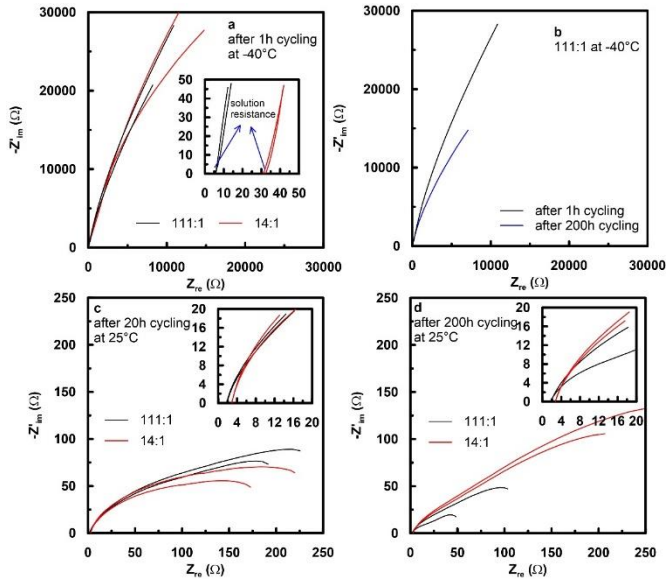

Fig. S18. Nyquist plots for Zn|Zn (100 μm) cells with selected electrolytes at different cycling time and different temperatures. a, After 1h cycling (0.125 mA cm^{-2}, 0.01 mAh cm^{-2} per-cycle) at -40° C; **b,** after 1h and 200h cycling (0.125 mA cm^{-2}, 0.01 mAh cm^{-2} per-cycle) for 111:1 electrolyte at -40° C; **c,** after 20h cycling (2.5 mA cm^{-2}, 2.5 mAh cm^{-2} per-cycle) at room temperature; **d,** after 200h cycling (2.5 mA cm^{-2}, 2.5 mAh cm^{-2} per-cycle) at room temperature. EIS data was measured at -40°C (a and b) and room temperature (c and d), respectively. Mild cycling conditions were applied at -40°C to make 14:1 electrolyte can be cycled in cells for EIS testing. The EIS testing frequency is from 100 kHz to 10 mHz.

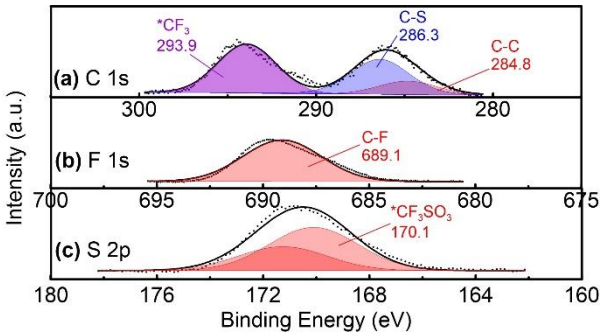

Fig. S19. XPS spectra of $Zn(OTf)_2$ salt. XPS spectra of **a,** C 1s,**b,**F 1s, and **c,** S 2p.

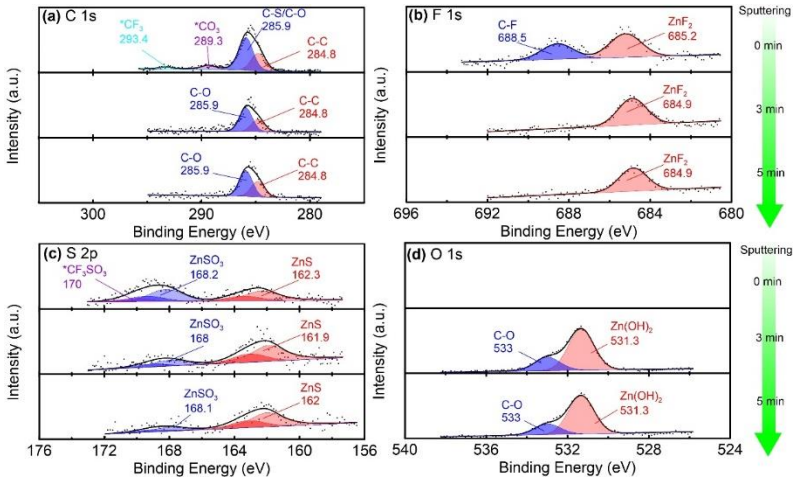

Fig. S20. Depth profile of XPS spectra. XPS spectra of **a,** C 1s, **b,** F 1s, **c,** S 2p , and **d,** O 1s for Zn metal. Ar^+ sputtering were conducted to generate depth profiles of C 1s, F 1s, S 2p and O 1s. Zn anode samples were obtained from Zn|Zn symmetric cells at zero state of charge after 20h cycling (2.5 mA cm^{-2},2.5 mAh cm^{-2} per cycle) with MeOH:$Zn(OTf)_2$ 14:1 by mol electrolyte at room temperature. O 1s spectra prior to sputtering is shown in Figure 3K.

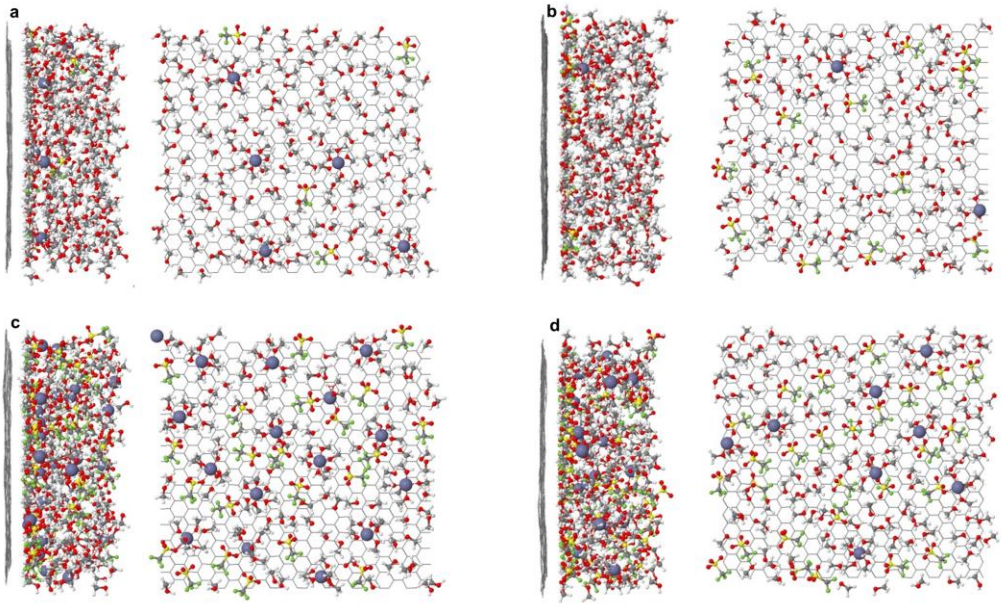

Fig. S21. A summary of image snapshot with side and frontal view of the electrode-electrolyte interface. a-b, MeOH:$Zn(OTf)_2$ 111:1 by mol electrolyte at **a,** negative potential and **b,** positive potential, respectively. **c-d,** MeOH:$Zn(OTf)_2$ 14:1 by mol electrolyte at **c,** negative potential and **d,** positive potential, respectively. Molecules were selected if their centers of geometry were within 8 Å widths from electrode. The electrode charge density was $|\sigma|$=5.36 $\mu C/cm^2$. The frontal view selected the molecules within 8Å from electrode while the side view selected molecules within 18Å from electrode.

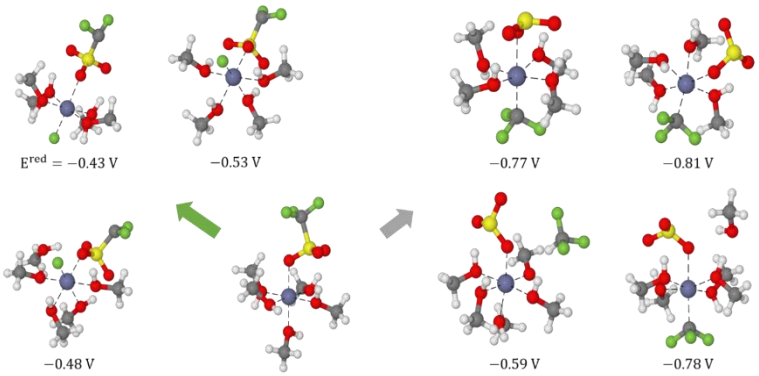

Fig. S22. DFT calculations on OTf^- anion reduction potential in a MeOH environment. Reduction potentials (in V vs Zn/Zn^{2+}) for $[ZnOTf(MeOH)_{4/5}]^+$ clusters. The green arrow points to a selection of defluorination products and the gray arrow to a few C-S cleavage products. Dashed black lines highlight the coordination of molecules around Zn. An explicit 5th methanol is included in some of these results, else, where you count 4 MeOH in the product, a 'bulk-like' contribution is considered instead (see Fig. S41).

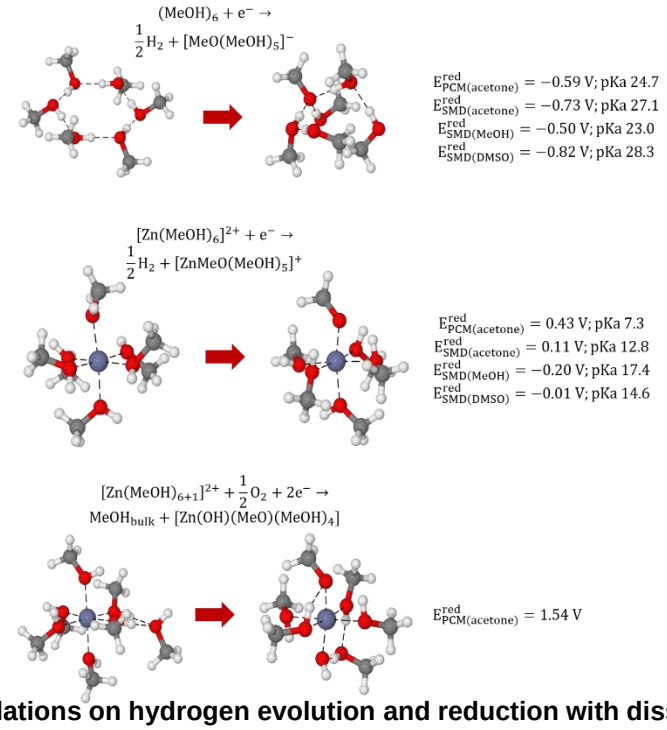

Fig. S23. DFT calculations on hydrogen evolution and reduction with dissolved oxygen in a MeOH environment. Reduction potentials (in V vs Zn/Zn^{2+}) for hydrogen evolution from methanol clusters (top) and $Zn(MeOH)_6$ cluster (middle). Potentials and pKa's are sampled with multiple solvation models and solvents. In general, protons are more acidic for Zn-coordinated MeOH. Reduction of Zn-coordinated MeOH with dissolved O_2 is considered as well as a precursor for evolution of $Zn(OH)_2$ (bottom). All calculations were performed at the M05-2X/6-311++G(3df,3pd) level of theory. $MeOH_{bulk}$ taken from Fig. S41.

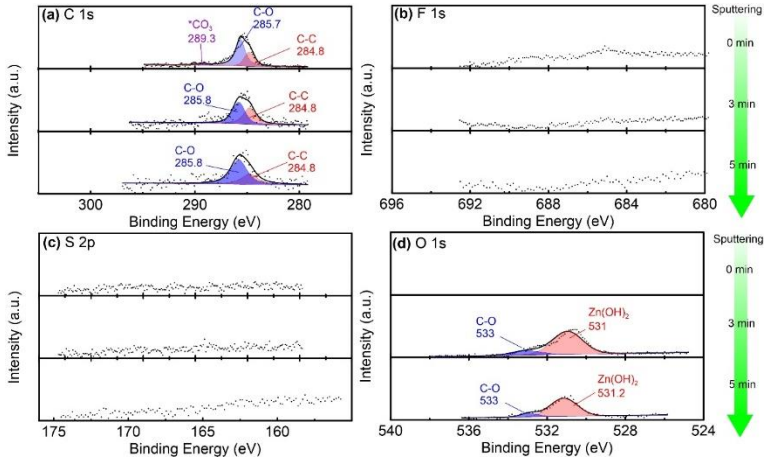

Fig. S24. Depth profile of XPS spectra. XPS spectra of **a,** C 1s, **b,** F 1s, **c,** S 2p, and **d,** O 1s for Zn metal. Ar^+ sputtering were conducted to generate depth profiles of C 1s, F 1s, S 2p and O 1s. Zn anode samples were obtained from Zn|Zn symmetric cells at zero state of charge after 20h cycling (2.5 mA cm^{-2},2.5 mAh cm^{-2} per cycle) with MeOH:$Zn(OTf)_2$ 111:1 by mol electrolyte at room temperature. O 1s spectra prior to sputtering is shown in Figure 3I.

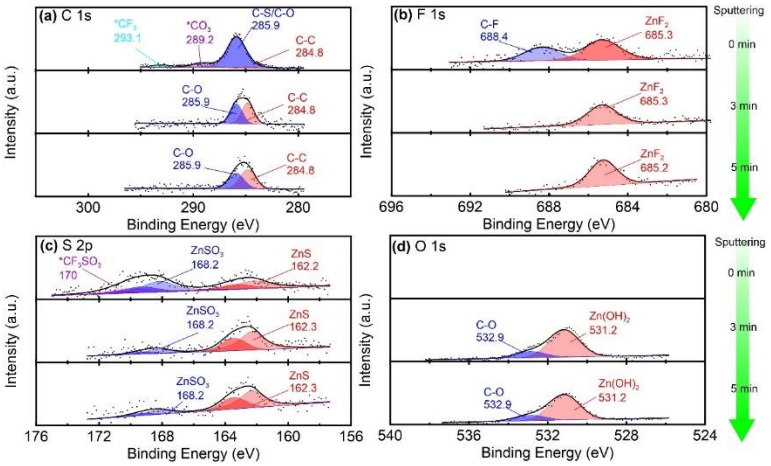

Fig. S25. Depth profile of XPS spectra. XPS spectra of **a,** C 1s, **b,** F 1s, **c,** S 2p, and **d,** O 1s for Zn metal. Ar^+ sputtering were conducted to generate depth profiles of C 1s, F 1s, S 2p and O 1s. Zn anode samples were obtained from Zn|Zn symmetric cells at zero state of charge after 200h cycling (2.5 mA cm^{-2},2.5 mAh cm^{-2} per cycle) with MeOH:$Zn(OTf)_2$ 111:1 by mol electrolyte at room temperature. O 1s spectra prior to sputtering is shown in Figure 3J.

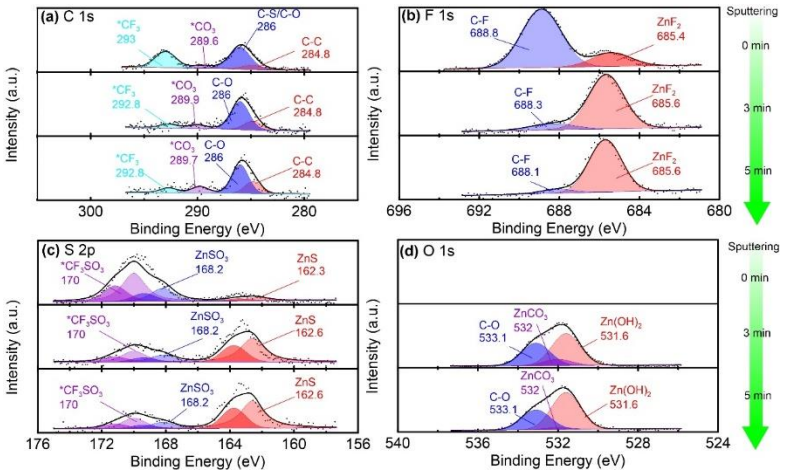

Fig. S26. Depth profile of XPS spectra. XPS spectra of **a,** C 1s, **b,** F 1s, **c,** S 2p, and **d,** O 1s for Zn metal. Ar^+ sputtering were conducted to generate depth profiles of C 1s, F 1s, S 2p and O 1s. Zn anode samples were obtained from Zn|Zn symmetric cells at zero state of charge after 200h cycling (2.5 mA cm^{-2},2.5 mAh cm^{-2} per cycle) with MeOH:$Zn(OTf)_2$ 14:1 by mol electrolyte at room temperature. O 1s spectra prior to sputtering is shown in Figure 3L.

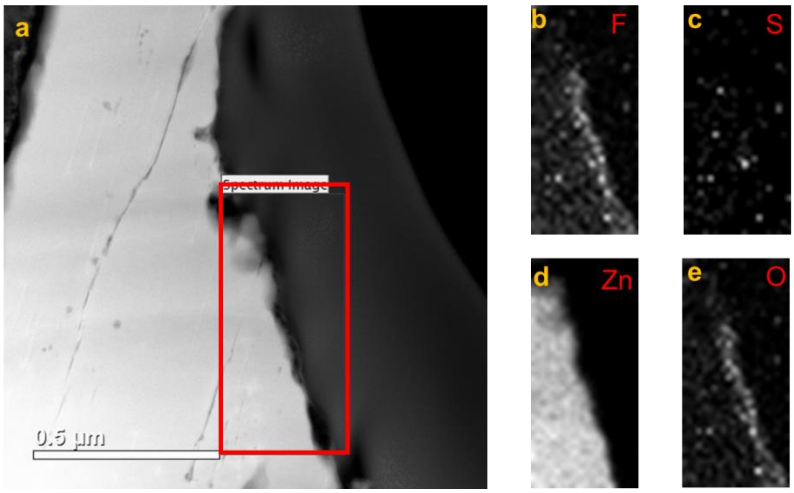

Fig. S27. Zn interphase morphology and chemistry during cycling. a, STEM HAADF mode observation of Zn metal with the evolved interphase layer. STEM EDS mapping area is indicated by the red rectangular box. **b-e,** EDS mapping of **b,** F, **c,** S, **d,** Zn, and **e,** O. Zn sample was obtained from Zn|Zn cells with MeOH:$Zn(OTf)_2$ 111:1 by mol electrolyte after 200h cycling (2.5 mA cm^{-2}, 2.5 mAh cm^{-2}) at zero state of charge.

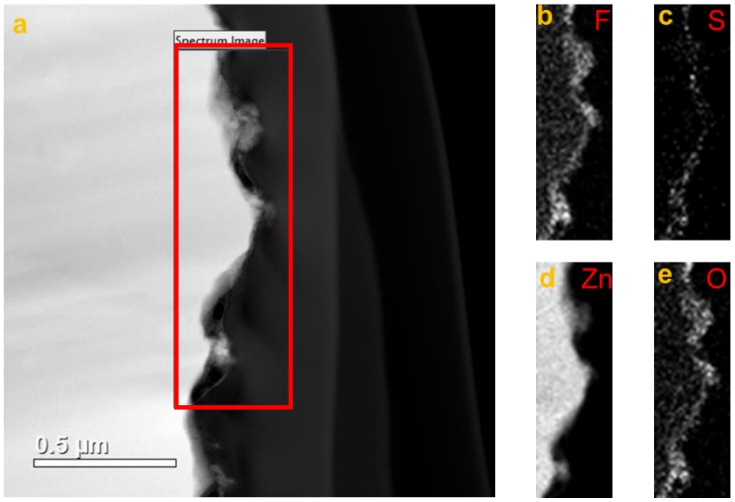

Fig. S28. Zn interphase morphology and chemistry during cycling. a, STEM HAADF mode observation of Zn metal with the evolved interphase layer. STEM EDS mapping area is indicated by the red rectangular box. **b-e,** EDS mapping of **b,** F, **c,** S, **d,** Zn, and **e,** O. Zn sample was obtained from Zn|Zn cells with MeOH:$Zn(OTf)_2$ 14:1 by mol electrolyte after 200h cycling (2.5 mA cm^{-2}, 2.5 mAh cm^{-2}) at zero state of charge.

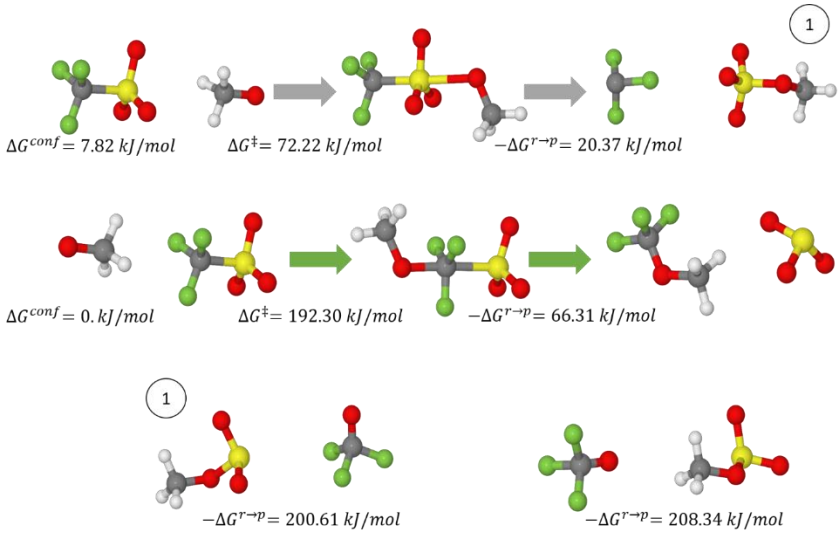

Fig. S29. Nucleophilic attack by methoxide on triflate, chemical decomposition in implicit solvent represented using PCM(acetone)/M05-2X/6-311++G(3df,3pd) method. Reactions considered include triflate with methoxide on the SO_3 side (top row) and CF_3 side (middle row). The interaction between methoxide and the CF_3 side is slightly favored (ΔG^{conf}). The barriers and reaction free energies are computed with respect to the reactant structures. The bottom row features two additional products related to the methoxide attack on the SO_3 group leading to the formation of trifluoromethoxide. Barrier for methoxide attack on the triflate anion and negative of the reaction free energy (difference reflects products – reactants) in kJ mol^{-1}.

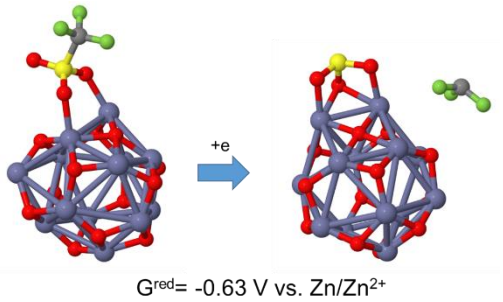

Fig. S30. DFT calculations on OTf^- anion reduction on a nano-scale ZnO cluster distributed on Zn metal surface using PCM(acetone)/M05-2X/6-31+G(d,p) method.

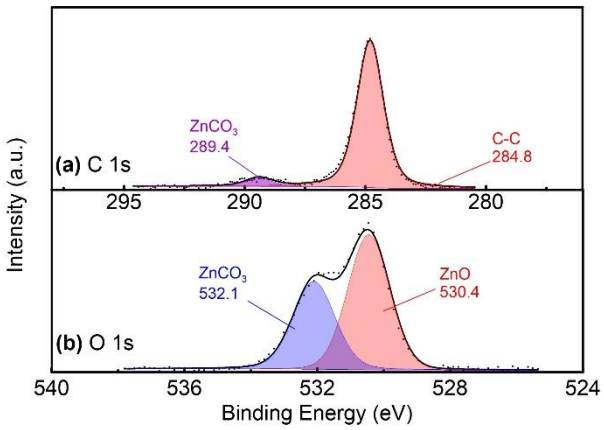

Fig. S31. XPS spectra of pristine Zn foil. XPS spectra of **a,** C 1s,and **b,** O 1s for a pristine Zn foil.

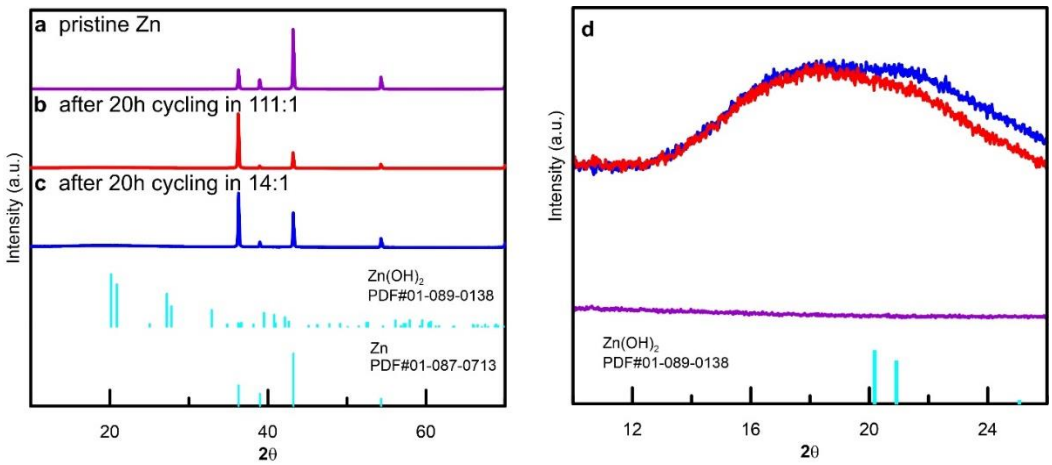

Fig. S32. XRD pattern of Zn metal electrodes. XRD pattern of **a,** pristine Zn foil, **b,** Zn metal electrodes after 20h cycling with 111:1 electrolyte, and **c,** Zn metal electrodes after 20h cycling with 14:1 electrolyte. **d,** A summary with an enlarged view for a-c. Zn metal anode samples for b and c were obtained from Zn|Zn symmetric cells at zero state of charge after 20h cycling (2.5 mA cm^{-2}, 2.5 mAh cm^{-2} per cycle) at room temperature.

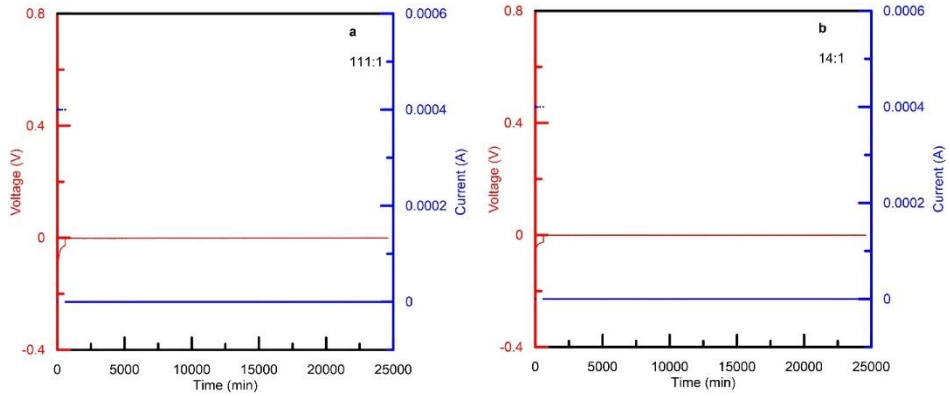

Fig. S33. Leakage/corrosion current testing with selected electrolytes during open circuit voltage condition at room temperature. a, 111:1 electrolyte,**b,** 14:1 electrolyte. Cu|Zn cells were discharged for 10h with 0.25 mA cm^{-2}. Then cell voltage and current were monitored during open circuit voltage condition at room temperature.

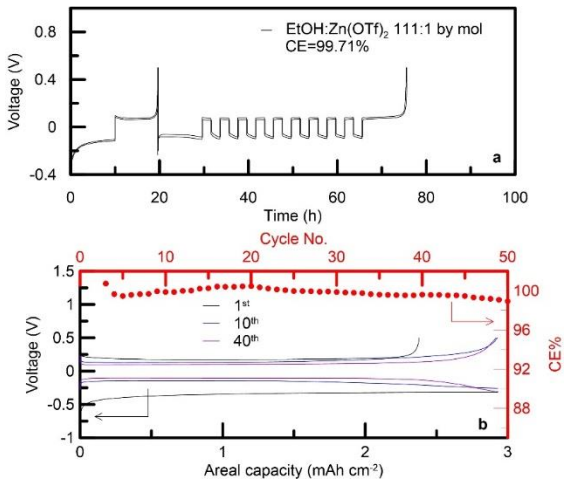

Fig. S34. Zn reversibility in EtOH:Zn(OTf)$_2$ 111:1 by mol electrolyte at room temperature. a, Voltage vs time for Cu|Zn (100 μm) cells at 25°C with selected electrolyte as labeled. Cu was conditioned by plating (0.5 mA cm^{-2}, 5 mAh cm^{-2}) and stripping Zn (0.5 V) during the first cycle. Then a Zn reservoir with a capacity of 5 mAh cm^{-2} was built on the Cu substrate using 0.5 mA cm^{-2}. 0.5 mA cm^{-2} was used for stripping and plating Zn during the following 9 cycles. A capacity of 1mAh cm^{-2} Zn was plated or stripped in each cycle. The cell was charged to 0.5 V to strip Zn during the last step. Calculated Zn plating/stripping CE were labeled in the panel. **b,** Zn plating/stripping profiles and corresponding CE using Cu|Zn(10 μm) cell setup with 2.93 mA cm^{-2}, 2.93 mAh cm^{-2} and 50% Zn utilization per cycle.

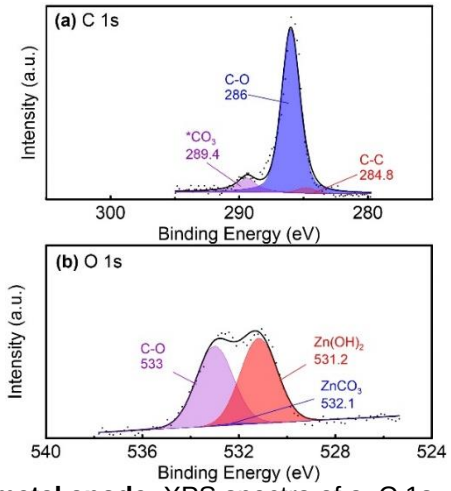

Fig. S35. XPS spectra on Zn metal anode. XPS spectra of **a,** C 1s, and **b,** O 1s for Zn metal. Zn anode samples were obtained from Zn|Zn symmetric cells at zero state of charge after 20h cycling (2.5 mA cm^{-2}, 2.5 mAh cm^{-2} per cycle) with EtOH:Zn(OTf)$_2$ 111:1 by mol electrolyte at room temperature.

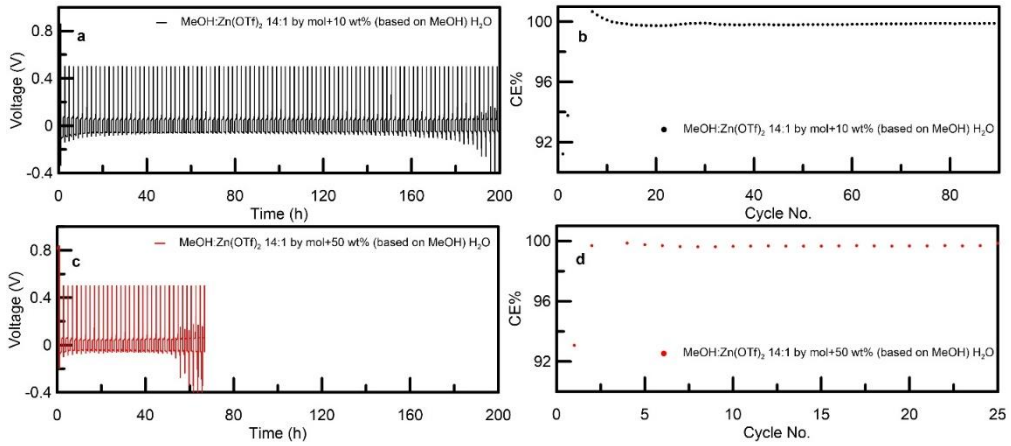

Fig. S36. The effect of water on Zn reversibility in MeOH:Zn(OTf)$_2$ 14:1 by mol electrolyte at room temperature. a, and **c,** Voltage vs time for Cu|Zn (10 μm) cells cycled with 2.93 mA cm^{-2}, 2.93 mAh cm^{-2} and 50% Zn utilization per cycle to plate Zn on Cu substrate, then charged to 0.5 V to strip Zn with different water content as labeled in each panel. Corresponding Zn stripping/plating CE for **a** and **c** are shown in **b** and **d**, respectively.

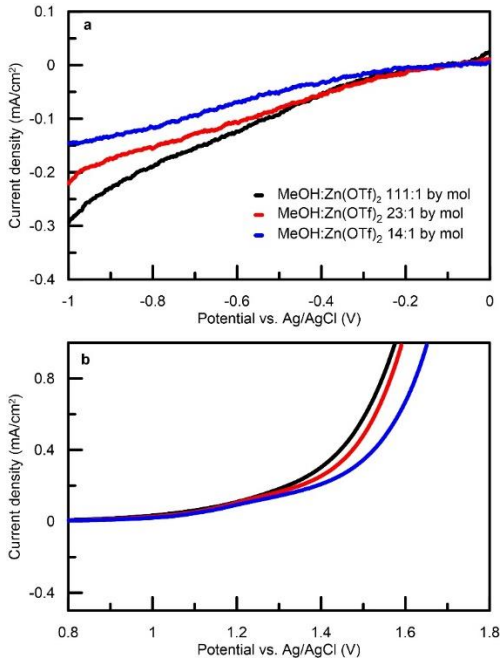

Fig. S37. Electrochemical stability analysis of the selected Zn electrolytes at room temperature. a, Cathodic region and **b,** anodic region during 2nd cycle. A three electrode Swagelok cell containing stainless steel (SS) as the working electrode, carbon black as the counter electrode and Ag/AgCl as the reference electrode was used for tesing at a scan rate of 5mV s^{-1} at room temperature.

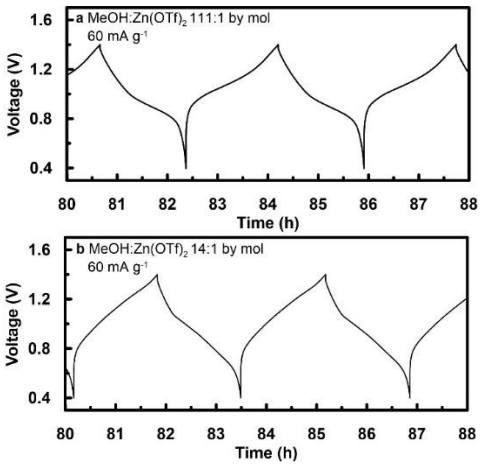

Fig. S38. Long-term cycling details at 30°C. Voltage vs time for PANI|Zn (10 μm) during long-term cycling at 30°C with different electrolytes as labeled. Corresponding cycling results have been shown in Figure 4. Each discharge step takes ~2h and corresponding areal capacity will be $60\ \frac{mA}{g} \times 7\ \frac{mg}{cm^2} \times 2h = 0.84 \frac{mAh}{cm^2}$. As a result, Zn utilization percentage per cycle will be $0.84 \frac{mAh}{cm^2} \div 5.85 \frac{mAh}{cm^2} = 14.4\%$.

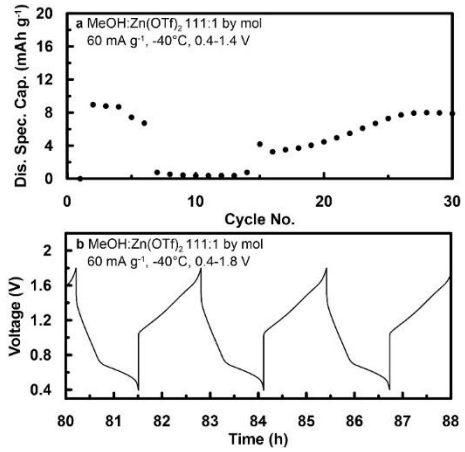

Fig. S39. Long-term cycling details at -40°C. a, Discharge specific capacity vs. cycle No. for a PANI|Zn (10 μm) cell tested at -40°C with 60 mA g^{-1} (based on the mass of PANI active material) between 0.4 and 1.4 V. **b,** Voltage vs time for a PANI|Zn (10 μm) cell tested at -40°C with 60 mA g^{-1} (based on the mass of PANI active material) between 0.4 and 1.8 V. Its corresponding cycling results have been shown in Figure 4E. The electrolytes used here are all MeOH:$Zn(OTf)_2$ 111:1 by mol. Each discharge step takes ~1.5h and corresponding areal capacity will be $60\ \frac{mA}{g} \times 7\ \frac{mg}{cm^2} \times 1.5h = 0.63 \frac{mAh}{cm^2}$. As a result, Zn utilization percentage per cycle will be $0.63 \frac{mAh}{cm^2} \div 5.85 \frac{mAh}{cm^2} = 11\%$.

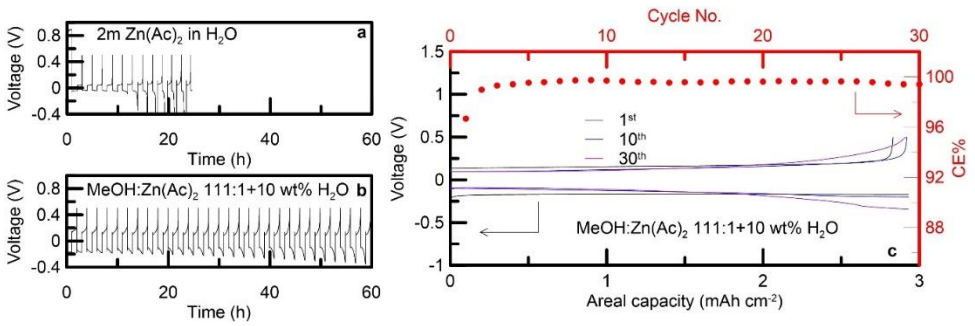

Fig. S40. Zn reversibility in green salt containing electrolyte at room temperature. Voltage vs time for Cu|Zn (10 μm) cells cycled with 2.93 mA cm^{-2}, 2.93 mAh cm^{-2} and 50% Zn utilization per cycle to plate Zn on Cu substrate, then charged to 0.5 V to strip Zn with different electrolytes: **a,** 2m $Zn(Ac)_2$ in H_2O; **b,** MeOH:$Zn(Ac)_2$ 111:1 by mole +10 wt% H_2O (based on the mass of MeOH). **c,** Zn plating/stripping profiles and corresponding CE for **b,**. The addition of 10 wt% H_2O is to facilitate the dissolution of $Zn(Ac)_2$ in MeOH.

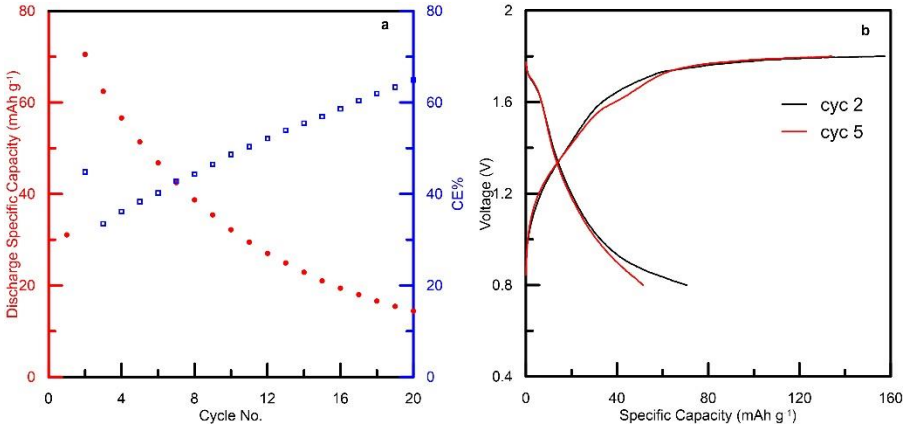

Fig. S41. Full cell performance demonstration of MeOH-based electrolytes. a, CE and corresponding specific discharge capacity vs. cycle number for 14:1 electrolyte tested with MnO_2 (~3 mg cm^{-2})|Zn(100 μm) cell setup at 50 mA g^{-1} (based on the mass of MnO_2) between 0.8 and 1.8 V at 30°C. **b,** Charge-discharge profile corresponding to the cell setup and electrolytes in **a,** .

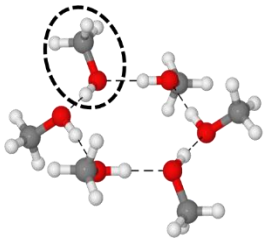

$$\approx \Delta G^{298}_{bulk}(MeOH)$$

Fig. S42. Methanol hexamer geometry used for estimating the free energy of methanol monomer in bulk methanol.

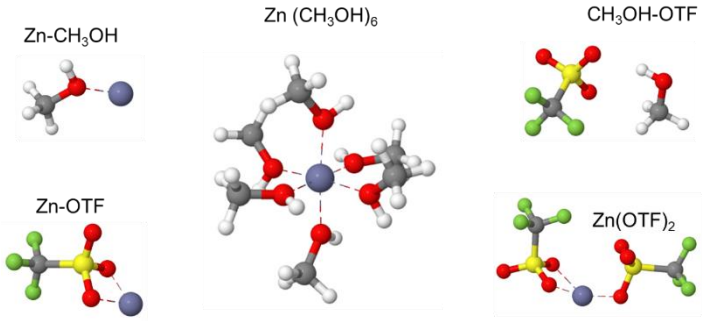

Fig. S43. Image snapshots of optimized clusters with molecular mechanics.

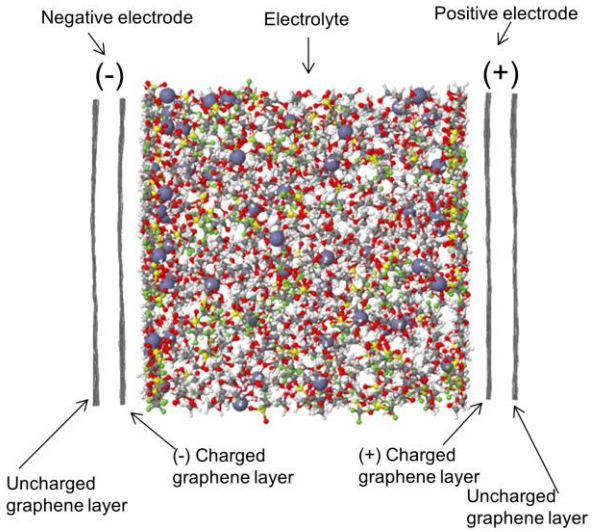

Fig. S44. Typical setup for the electrode-electrolyte simulations, consisting of an electrolyte confined between two oppositely charged electrodes.

Table S1. Summary of Zn metal anode reversibility in selected state-of-art Zn electrolyte at room temperature or low temperature (<0°C). The name of aqueous electrolytes is labeled **in bold**.

Electrolyte	Temperature	Claimed CE	Zn utilization per-cycle	Plating areal capacity per-cycle	Plating current density	Lifetime
This work (MeOH:$Zn(OTf)_2$ 111:1 by mol)	25°C	>99.9%	50%	2.93 mAh cm^{-2}	2.93 mA cm^{-2}	>280h
This work (MeOH:$Zn(OTf)_2$ 111:1 by mol)	-40°C	>99.5%	20%	1.17 mAh cm^{-2}	1.17 mA cm^{-2}	>540h
0.5M Zn(OTf)2 in TEP(13)	25°C	99.68%	0.34%	0.5 mAh cm^{-2}	0.5 mA cm^{-2}	2000h
0.5M Zn(OTf)2 in TMP(14)	25°C	99.57%	N/A	0.5 mAh cm^{-2}	0.5 mA cm^{-2}	1000h
$Zn(TFSI)_2$/acetamide 1/7 (by mol)(15)	25°C	>98%	N/A	1 mAh cm^{-2}	0.5 mA cm^{-2}	40h
1M $Zn(TFSI)_2$ in AN(16)	25°C	99.8%	N/A	0.1 mAh cm^{-2}	0.2 mA cm^{-2}	200h
$Zn(ClO_4)_2$•$6H_2O$/SN (1/8 by mole)(17)	25°C	98.4%	N/A	0.5 mAh cm^{-2}	0.5 mA cm^{-2}	180h
0.5M $Zn(OTf)_2$ in DMF(18)	25°C	~100%	5.7%	1 mAh cm^{-2}	1 mAh cm^{-2}	400h
2M $ZnSO_4$ in H_2O/MeOH (1/1 by vol.)(19)	25°C	99.3%	N/A	0.5 mAh cm^{-2}	1 mA cm^{-2}	900h
2M $ZnSO_4$ in H_2O/MeOH (1/1 by vol.)(19)	-10°C	99.5%	N/A	0.5 mAh cm^{-2}	1 mA cm^{-2}	200h
7.5 m $ZnCl_2$ in water(20)	-70°C	99.52%	N/A	0.2 mAh cm^{-2}	0.2 mA cm^{-2}	450h
2M $ZnSO_4$ in H_2O/ethylene glycol (5/2 by vol.)(21)	25°C	98%	3.4%	1 mAh cm^{-2}	2 mA cm^{-2}	130h
2M $ZnSO_4$ in H_2O/ethylene glycol (5/2 by vol.)(21)	-20°C	99%	3.4%	1 mAh cm^{-2}	2 mA cm^{-2}	60h

Table S2. Summary of MD simulation results on H-bond in different electrolytes. The H-bond network between H-O of CH_3OH was assessed with the following criterion: if two non-bonded H and O belonging to CH_3OH were within a distance of 2.4 Å (which encompasses the 1st peak in density profiles), then they were considered as H bonded.

Electrolyte	H-bond number per MeOH
Pure MeOH solvent	2
MeOH:$Zn(OTf)_2$ 111:1 by mol	1.8
MeOH:$Zn(OTf)_2$ 14:1 by mol	1.3

Table S3. A summary of MD simulations of $Zn(OTf)_2$ in MeOH at 60 °C.

Prop/system	MeOH:Zn=111:1	MeOH:Zn=14:1
Trajectory length(ns)	23.6	57.05
Box-size(Å)	63.51	41.67
Density(g/cm^3)	0.8132	1.1926
Composition of the simulation box	3552 (MeOH) 64 (OTf) 32 (Zn)	896 (MeOH) 128 (OTf) 64 (Zn)
Coordination number for Zn-O(OTf) within 3.0 Å	0.08	0.28
Coordination number for Zn-O(MeOH) within 3.0 Å	5.91	5.70
D(Zn) (10^{-10} m^2 s^{-1})	7.9	0.62
D(OTf) (10^{-10} m^2 s^{-1})	10.7	1.08
D(MeOH) (10^{-10} m^2 s^{+1})	29.1	3.45
t_+ (Zn^{2+})	0.5	0.4
Viscosity (mPa*s)	0.53	7.3
Conductivity (mS cm^{-1})	19.6	11.0
α_d, Ionicity	0.53	0.48

Table S4. Summary of cell energy density estimation for Figure 4 at 30°C. The calculation is based on the following parameters (separator, electrolyte and current collectors are not considered for this calculation): specific discharge capacity (100 mAh/g_{PANI}), average voltage (~1 V), cathode active material mass (7 mg cm^{-2}), cathode material thickness (~35 μm), Zn anode mass (7.13 mg cm^{-2}), Zn anode thickness (10 μm).

Volumetric energy density (Wh L^{-1})
158

Table S5. A summary of estimated cost (per kg) for selected state-of-art electrolytes. Zn salt price data is referred to a previous report(22). Laboratory-grade MeOH is available in commercial quantities (i.e. 55 gallon drum) at an estimated cost of $6/kg. The price of water is negligible.

Electrolyte	Estimated cost (per kg)	Note
This work: MeOH:$Zn(OTf)_2$ 111:1 by mol	$33.2	
This work: MeOH:$Zn(OTf)_2$ 14:1 by mol	$137.8	
20m LiTFSI+1m $Zn(TFSI)_2$ in H_2O(23)	$9599	The price of LiTFSI is estimated as $9230/kg according to Sigma Aldrich.
30m $ZnCl_2$ in H_2O(24)	$51	
0.5M Zn(OTf)2 in TEP(13)	$123.4	The price of TEP is estimated as $100/L according to Sigma Aldrich.
0.5M Zn(OTf)2 in TMP(14)	$648	The price of TMP is estimated as $700/kg according to Sigma Aldrich.
0.5M $Zn(OTf)_2$ in DMF(18)	$153	The price of DMF is estimated as $117/L according to Sigma Aldrich.
$Zn(ClO_4)_2$•$6H_2O$/SN (1/8 by mole)(17)	$684.7	The price of SN is estimated as $788/kg according to Sigma Aldrich.

Table S6. Binding energies of various clusters in vacuum calculated with molecular mechanics (MM) using developed force field and quantum chemistry (QC). The energies are in kJ mol^{-1}, QC method is given in parenthesis, Tz denotes aug-cc-pvTz basis set.

cluster	Zn-OTf	$Zn(OTf)_2$	CH_3OH-OTf	Zn-CH_3OH	$Zn(CH_3OH)_6$
MM energy	-1480.72	-2187.81	-48.53	-484.09	-1575.28
QC energy	-1476.12 (CBS-QB3)	-2271.91 (CBS-QB3)	-52.72 (ωB97XD/6-311+G(2df,2p)) -11.3 (G4MP2)	-487.85 (CCSD/Tz //MP2/Tz) -117.5 (ωB97XD/6-311+G(2d,2p)	-1559.38 (ωB97XD/6-311+G(2d,2p))

Table S7. The revised OTF^- parameters used in MD simulations of MeOH/$Zn(OTf)_2$ electrolytes.

a, Atom definitions added to amoeba09.prm

Type	Class	Symbol	Comment	Z	Mass	Valence
385	120	S	"S of OTF"	16	32.066	4
386	121	O	"O of OTF"	8	15.999	1
387	122	C	"C of OTF"	6	12.011	4
388	123	F	"F of OTF"	1	18.998	1

b, Parameters for the Halgren buffered 14-7 potential describing van der Waals (vdW) interactions added to amoeba09.prm

Class 1	Class 2	Sigma	Epsilon (kcal mol^{-1})
120	120	4.0100	0.5050
121	121	3.7100	0.3120
122	122	3.9700	0.2910
123	123	3.3500	0.3200
13	120	4.25	0.22
13	121	3.0	0.21

c, Multipoles interactions added to amoeba09.prm in units of electron (e) and bohr.

Multipole atoms Triplet: i j k	Parameters q (e), px,py.pz (e bohr, qxx qyy qxy qxz qyz (e $bohr^2$)
multipole 385 0 0	1.990911276 -0.20068 -0.1580550 0.317250 -0.525145 -0.933555 -0.1274000 0.4163700 0.70218
multipole 386 385 386	-0.7926637586 0.02310 -0.01162 -0.54130 0.19767 0.20917 -0.56684 -0.11237 0.24182
multipole 387 385 388	0.24770 -0.05703 0.17665 -0.96854 1.05238 1.46046 -0.46075 -0.40667 0.66266
multipole 388 387 385	-0.26354 0.07764 -0.00542 0.07140 0.36711 -0.38611 0.11638 0.32857 0.13

d, Polarizabilities added to amoeba09.prm

Type	Polarizability ($Å^3$)	Thole	pole in group
385	3.000	0.39	386
386	0.935	0.39	385
387	1.340	0.39	388
388	0.445	0.39	387

Supplementary Note on Extracting Transport Properties from MD Simulations

Methodology for extracting transport properties from MD simulations follows previous work,(25) and is described below for completeness. Solvent and ion self-diffusion coefficients were extracted using the Einstein relation from linear fits to mean-square displacements divided by six. Viscosity was calculated using the Einstein relation including both diagonal and non-diagonal elements to enhance the statistics using eqs S3-S5:

$$\eta = \lim_{t\to\infty} \eta(t) = \lim_{t\to\infty} \frac{V}{20k_B Tt}\left\langle \sum_{\alpha,\beta} \left(L_{\alpha\beta}(t) - L_{\alpha\beta}(0)\right)^2 \right\rangle \qquad \text{(S3)}$$

$$L_{\alpha\beta}(t) = \int_0^t P_{\alpha\beta}(t')\, dt' \qquad \text{(S4)}$$

where k_B is the Boltzmann constant, T is temperature, t is time, V is the volume of the simulation box, P_{ab} is the stress sensor given by:

$$P_{\alpha\beta} = \frac{\sigma_{\alpha\beta} + \sigma_{\beta\alpha}}{2} - \frac{\delta_{\alpha\beta}}{3} tr(\sigma) \qquad \text{(S5)}$$

where σ_{ab} is the stress tensor with $\delta_{ab} = 1$ for $\alpha = \beta$ and $\delta_{ab} = 0$ for $\alpha \neq \beta$.
The dynamic degree of ion uncorrelated motion (α_d) was calculated eqs. S6-S8:

$$\alpha_d = \frac{\kappa}{\kappa_{uncorr.}} \qquad \text{(S6)}$$

$$\kappa_{uncorr} = \frac{e^2}{Vk_B T}(n_+ D_+ + n_- D_-) \qquad \text{(S7)}$$

$$\kappa = \lim_{t\to\infty} \frac{e^2}{6tVk_B T} \sum_{i,j}^{N} z_i z_j < ([\mathbf{R}_i(t) - \mathbf{R}_i(0)])([\mathbf{R}_j(t) - \mathbf{R}_j(0)]) > \qquad \text{(S8)}$$

where e is the electron charge, V is the volume of the sample, k_B is Boltzmann's constant, T is the temperature and n_+ and n_- are the number of cations and anions, respectively. κ_{uncorr} is the "ideal" conductivity that would be realized if ion motion were uncorrelated.
Low value of ion uncorrelated motion (ionicity) at 111:1 of 0.53 (see Table S2) despite high Zn-OTF dissociation (89% of Zn% are solvent separated from OTF) indicates strong correlation of Zn and OTF motion even when they are separated by solvent.

SI References

1. Ma L, *et al.* (2020) Critical Factors Dictating Reversibility of the Zinc Metal Anode. *ENERGY & ENVIRONMENTAL MATERIALS* 3(4):516-521.
2. Zhao Y, Schultz NE, & Truhlar DG (2006) Design of Density Functionals by Combining the Method of Constraint Satisfaction with Parametrization for Thermochemistry, Thermochemical Kinetics, and Noncovalent Interactions. *Journal of Chemical Theory and Computation* 2(2):364-382.
3. Malloum A, Fifen JJ, & Conradie J (2018) Solvation energies of the proton in methanol revisited and temperature effects. *Physical Chemistry Chemical Physics* 20(46):29184-29206.
4. Frisch MJ, *et al.* (2016) Gaussian 16 Rev. C.01Wallingford, CT).
5. Larsen AH, *et al.* (2017) The atomic simulation environment—a Python library for working with atoms. *Journal of Physics: Condensed Matter* 29(27):273002.
6. Hanwell MD, *et al.* (2012) Avogadro: an advanced semantic chemical editor, visualization, and analysis platform. *Journal of Cheminformatics* 4(1):17.
7. Halgren TA (1996) Merck molecular force field. I. Basis, form, scope, parameterization, and performance of MMFF94. *Journal of Computational Chemistry* 17(5-6):490-519.
8. Borodin O, Olguin M, Spear CE, Leiter KW, & Knap J (2015) Towards high throughput screening of electrochemical stability of battery electrolytes. *Nanotechnology* 26(35):354003.
9. Bryantsev VS (2013) Predicting the stability of aprotic solvents in Li-air batteries: pKa calculations of aliphatic C–H acids in dimethyl sulfoxide. *Chemical Physics Letters* 558:42-47.
10. Kelly CP, Cramer CJ, & Truhlar DG (2007) Single-Ion Solvation Free Energies and the Normal Hydrogen Electrode Potential in Methanol, Acetonitrile, and Dimethyl Sulfoxide. *The Journal of Physical Chemistry B* 111(2):408-422.
11. Tomberli B, Egelstaff PA, Benmore CJ, & Neuefeind J (2001) Isotopic quantum effects in the structure of liquid methanol: I. Experiments with high-energy photon diffraction. *J. Physics: Condensed Matter* 13(50):11405-11420.
12. Galicia-Andrés E, Pusztai L, Temleitner L, & Pizio O (2015) Microscopic structure of methanol–water mixtures: Synchrotron X-ray diffraction experiments and molecular dynamics simulations over the entire composition range. *J. Mol. Liq.* 209:586-595.
13. Naveed A, Yang H, Yang J, Nuli Y, & Wang J (2019) Highly Reversible and Rechargeable Safe Zn Batteries Based on a Triethyl Phosphate Electrolyte. *Angewandte Chemie International Edition* 58(9):2760-2764.
14. Naveed A, *et al.* (2019) A Highly Reversible Zn Anode with Intrinsically Safe Organic Electrolyte for Long-Cycle-Life Batteries. *Advanced Materials* 31(36):1900668.
15. Qiu H, *et al.* (2019) Zinc anode-compatible in-situ solid electrolyte interphase via cation solvation modulation. *Nature Communications* 10(1):5374.
16. Zhang N, *et al.* (2019) Ultrafast Rechargeable Zinc Battery Based on High-Voltage Graphite Cathode and Stable Nonaqueous Electrolyte. *ACS Applied Materials & Interfaces* 11(36):32978-32986.
17. Yang W, *et al.* (2020) Hydrated Eutectic Electrolytes with Ligand-Oriented Solvation Shells for Long-Cycling Zinc-Organic Batteries. *Joule* 4(7):1557-1574.

18. Wang N, *et al.* (2020) Zinc–Organic Battery with a Wide Operation-Temperature Window from −70 to 150 °C. *Angewandte Chemie International Edition* 59(34):14577-14583.
19. Hao J, *et al.* (2021) Boosting Zinc Electrode Reversibility in Aqueous Electrolytes by Using Low-Cost Antisolvents. *Angewandte Chemie International Edition* 60(13):7366-7375.
20. Zhang Q, *et al.* (2020) Modulating electrolyte structure for ultralow temperature aqueous zinc batteries. *Nature Communications* 11(1):4463.
21. Chang N, *et al.* (2020) An aqueous hybrid electrolyte for low-temperature zinc-based energy storage devices. *Energy & Environmental Science* 13(10):3527-3535.
22. Han D, *et al.* (2021) A non-flammable hydrous organic electrolyte for sustainable zinc batteries. *Nature Sustainability*.
23. Wang F, *et al.* (2018) Highly reversible zinc metal anode for aqueous batteries. *Nature Materials* 17(6):543-549.
24. Zhang C, *et al.* (2018) A ZnCl2 water-in-salt electrolyte for a reversible Zn metal anode. *Chemical Communications* 54(100):14097-14099.
25. Borodin O & Smith GD (2009) Quantum Chemistry and Molecular Dynamics Simulation Study of Dimethyl Carbonate: Ethylene Carbonate Electrolytes Doped with LiPF6. *J. Phys. Chem. B* 113(6):1763-1776.